A Comparative Study of the Signal to Noise Ratio of Received Signals in a Reverberation Chamber and an Anechoic Chamber

Andrew C. Marvin
School of Physics, Engineering and Technology
University of York
York, UK.
andy.marvin@york.ac.uk

Simon J. Bale
School of Physics, Engineering and Technology
University of York
York, UK
simon.bale@york.ac.uk

Ian D. Flintoft
Electrical Systems
SNC-Lavalin/Atkins
York, UK
ian.flintoft@atkinsglobal.com

***Abstract*—The received signal and thermal noise characteristics of radiated emission measurements made in a reverberation chamber and an anechoic chamber are estimated over the frequency range from 1 GHz to 10 GHz. The contributions of the different elements of the receiving system in the reverberation chamber to the overall signal to noise ratio are illustrated and the consequences of these are shown for the detection of low-level signals.**

Keywords—signal to noise ratio, reverberation chamber, anechoic chamber

I. Introduction

Reverberation chambers are used for a number of purposes in Electromagnetic Compatibility (EMC) measurements as described in [1]. The measurement of radiated power from an Equipment-under-Test (EUT) is described in [1]. The equivalent standard for anechoic chambers is described in [2]. At low radiated power levels, the smallest signal that can be measured is limited by the signal to noise ratio (SNR) determined by the noise performance of the receiving system. This has implications for the search and detection of low-level signals. In [3] it was shown that the contribution of the reverberation chamber to this thermal noise depends on the mis-match factor of the receiving antenna in the reverberation chamber. In [4] it was shown that the SNR depends on both on the position of the rotating stirrer (and by implication, any other mechanical stirring device) and on the position and orientation of the EUT in the working volume of the reverberation chamber. All the measurements in [3] and [4] were taken at a single frequency of 800 MHz. This was the frequency that gave the lowest system input noise temperature in the available measurement system.

In this paper we extend the study of the received SNR in a reverberation chamber across a decade frequency range from 1 GHz to 10 GHz to illustrate how the contributions to the SNR by the different components in the receiving system are made. The limits of the possible range of SNR over the frequency range are investigated. The reverberation chamber results are compared to the equivalent anechoic chamber results for the same EUT, receiving antenna and transmitted power. In Section II the thermal noise characteristics of a reverberation chamber are reviewed. Section III describes how these noise characteristics can be estimated from Vector Network Analyser (VNA) measurements alone. Section IV describes measurements and calculations comparing the signal and noise characteristics of both a reverberation chamber and an anechoic chamber based on measurement techniques described in [1] and [2].

II. Antenna Noise Temperature in a Reverberation Chamber

In Fig. 1, reproduced from [3], the basic receiving system is shown. The EUT is placed in the chamber and the receiving antenna receives the some of the radiated power from the EUT along with thermal noise generated by the structure of the chamber, the stirrer and the receiving antenna internal loss (efficiency) represented here by the antenna noise temperature T_{ant}. Added to the thermal noise from the chamber is the internal noise of the receiving system represented by the antenna noise temperature T_{sys}, or equivalently by the Noise Figure (NF) of the receiving system.

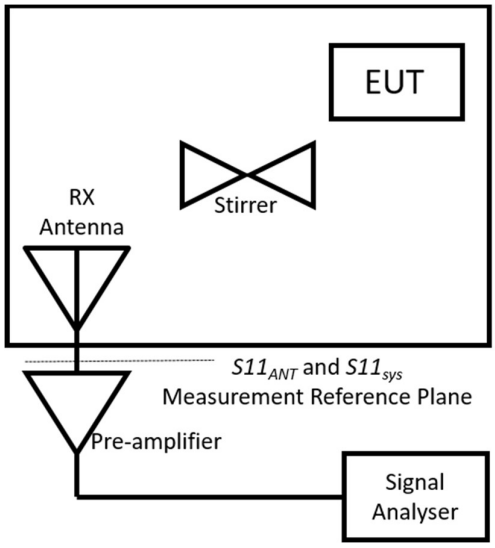

Fig. 1. Reverberation chamber receiving system.

In this investigation it was found more convenient to represent the receiver noise contribution in terms of a receiving system input noise temperature, T_{sys}. This is related to the NF by

$$NF = 10log_{10}\left(1 + \frac{T_{sys}}{290}\right)\ dB \qquad (1)$$

The NF is defined for a standard noise temperature of 290 K. The total input noise power to the receiving system is then

$$N_{RX} = \left(T_{sys} + T_{ant}\right)kB \quad \text{[watt]} \qquad (2)$$

where k is Boltzman's constant and B is the receiver resolution bandwidth.

In [3] the mis-match correction ratio C was defined by

$$C = \frac{(1-|S11_{ant}|^2)}{|1-S11_{ant}S1_{\ sys}|^2} \quad (3)$$

where $S11_{ant}$ is the receiving antenna input scattering parameter measured using a VNA and $S11_{sys}$ is the input scattering parameter of the receiving system. As the stirrer is rotated the value of $S11_{ant}$ changes thereby changing the mismatch correction ratio C.

In [3] the linear relationship between the mis-match correction ratio C and the apparent receiving antenna noise temperature was demonstrated with a Pearson linear correlation coefficient of 0.96. This is shown here in Fig. 2, reproduced from [3]. Each point in the cloud in Fig. 2 relates to one of four hundred stirrer positions. The ambient temperature of the chamber structure was 301 K at the time this measurement was taken and this temperature is indicated in Fig. 2 for a C value of 1. In general, the apparent antenna noise temperature is less than the ambient temperature of the chamber structure by a factor equal to the mis-match correction ratio. Note however that C can have a value above unity at some stirrer positions indicating that the apparent antenna noise temperature is above the ambient temperature. This is due to the antenna presenting a better conjugate impedance match to the receiver than the impedance match of a 50 Ω load to the receiver.

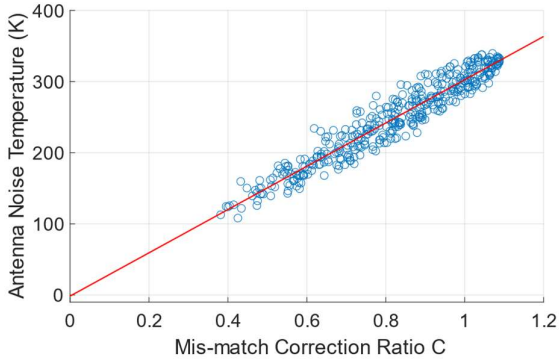

Fig. 2. Linear relationship between the antenna noise temperature and the mis-match correction ratio C

This linear relationship between the antenna noise temperature and the mis-match correction ratio C enables a parametric study of the SNR characteristics of the reverberation chamber / receiver measurement system to be undertaken without the requirement to measure noise. All aspects of the system noise performance can be derived from VNA measurements and defined values of the ambient temperature, the receiver resolution bandwidth and the receiver input noise temperature. For a chamber structure ambient temperature T_{amb} the apparent antenna noise temperature T_{ant} in (2) becomes

$$T_{ant} = CT_{amb} \quad (4)$$

III. Network Analyser Derived Reverberation Chamber Signal and Noise Characteristics

For simplicity in this illustrative study the VNA was used to provide signal power to the EUT (in this case a biconical dipole antenna described in Section IV) and as the receiving system as shown in Fig. 3. In these circumstances, the receiver system was assumed to be perfectly matched and the value of $S11_{sys}$ is zero. The chamber mis-match correction ratio C then becomes

$$C = 1 - |S11_{ant}|^2 \quad (5)$$

and the maximum antenna noise temperature is the ambient temperature of the chamber structure achieved if $S11_{ant}$ is zero, i.e. the antenna presents a matched load. Under these circumstances the maximum value of C is 1 when the antenna is conjugate impedance matched to the receiver (VNA). In principle, any receiver input mis-match could be incorporated into the study.

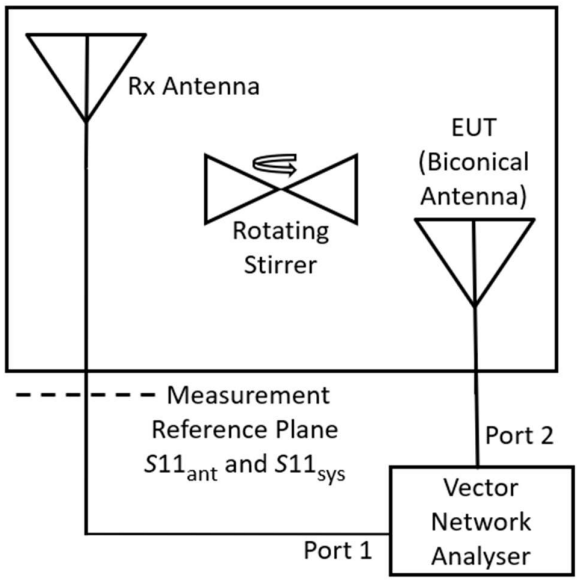

Fig. 3. Reverberation chamber measurements system using the VNA

In this matched case, the total noise present at the input to the receiver is derived by combining (2), (4) and (5) to give

$$N_{RX} = \left(T_{sys} + (1 - |S11_{ant}|^2)T_{amb}\right)kB \text{ [watt]} \quad (6)$$

The power received by the Rx antenna from the EUT with a transmitted power of P watts is S_{RX},

$$S_{RX} = |S21|^2 P \text{ [watt]} \quad (7)$$

Thus by measuring the scattering parameters in the reverberation chamber and defining the ambient temperature, the system noise temperature, the resolution bandwidth and the power presented to the EUT, the signal to noise characteristics of the measurement can be estimated and explored.

IV. Signal to Noise Ratio Estimates with a Biconical Dipole Antenna Equipment Under Test

A small biconical antenna was used as a simple EUT. It is shown mounted in the reverberation chamber in Fig. 4.

Fig. 4. Biconical dipole antenna EUT in the reverberation chamber

The receiving antenna was a 1 GHz – 18 GHz ETS 3115 ridged waveguide horn antenna shown in Fig. 5 mounted in the reverberation chamber.

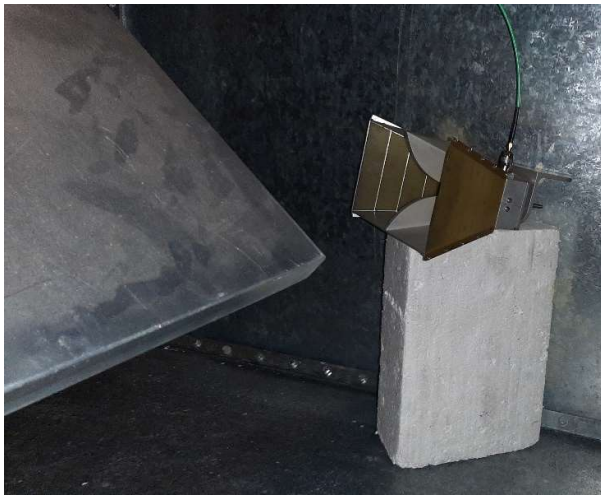

Fig. 5. Ridged waveguide horn antenna type ETS 3115 mounted in the reverberation chamber, also showing part of the stirrer

Fig. 6 shows the maximum and minimum values of $|S21|$ in the frequency range 1 GHz to 10 GHz at 1 MHz intervals. Four hundred stirrer positions were used in one rotation of the stirrer. Also shown in Fig. 6, annotated "Mean", is the average chamber insertion loss $\langle|S21|\rangle$, where $\langle\rangle$ denotes the average over all stirrer positions.

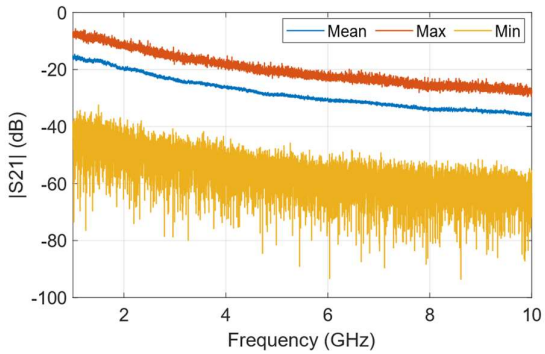

Fig. 6. Maximum and minimum $|S21|$ and the chamber insertion loss (Mean)

The maximum and minimum values of $|S21|^2$ indicate the range of received powers over the four hundred stirrer positions through (7). This power range remains substantially constant over the frequency range. In Fig. 7 the range of the receiving antenna reflection coefficient, $S11$, over the four hundred stirrer positions is shown along with the vector mean of these, which gives the antenna free space reflection coefficient. At the lower frequencies the antenna is not well matched. In Fig. 8 the range of the mis-match correction ratio C is shown. These data determine the total receiver input noise power N_{RX} for a chosen resolution bandwidth B, system noise temperature T_{sys}, and ambient temperature T_{amb} through (6). These data are shown in Fig. 9 for an ambient temperature of 290 K, a low noise receiving system with an input noise temperature of 40 K and a measurement bandwidth of 10 kHz.

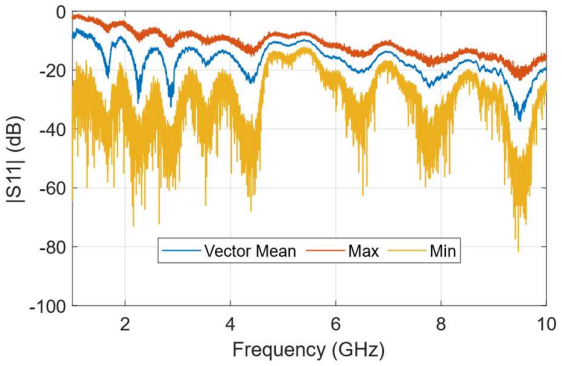

Fig. 7. Variability of the receiving antenna reflection coefficient and its vector mean

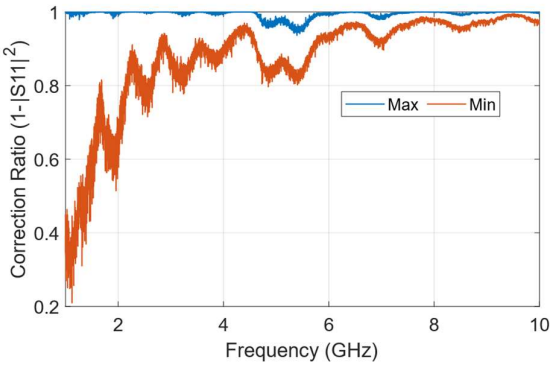

Fig. 8. Maximum and minimum mis-match correction ratios C

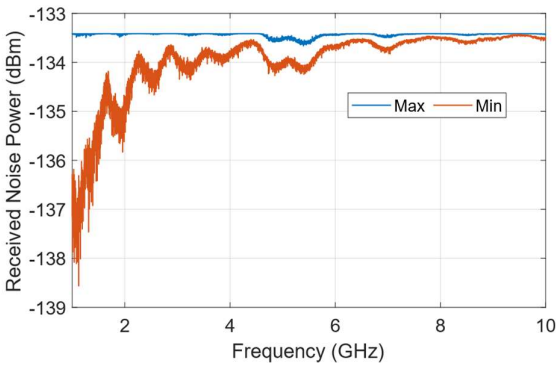

Fig. 9. Maximum and minimum total noise power at the receiver input

A. Signal received in an anechoic chamber

In order to compare the results in a reverberation chamber with those obtained in an equivalent anechoic chamber measurement the transmitted powers required to give 0 dB SNR were calculated for the anechoic chamber measurement. In an anechoic chamber the antenna noise temperature is the ambient temperature of the chamber walls. The transmitted power required to achieve a received power equal to the receiver input noise power (0 dB SNR) can be calculated using (8), derived from the Friis equation [5]. For simplicity, perfectly matched transmitting and receiving antennas with gains G_{tx} and G_{rx} respectively were assumed. At an antenna to antenna separation R, frequency denoted by the associated wavelength λ, transmitted power P and measurement bandwidth B the received signal power equals the noise power when

$$k(T_{sys} + T_{amb})B = {}^{PG_{tx}G_{rx}\lambda^2}/_{16\pi^2R^2} \qquad (8)$$

Assume a typical anechoic chamber measurement set-up comprising a separation distance of 3m, a dipole transmitting antenna with gain 1.64 as the EUT, a ridged waveguide horn receiving antenna, an ambient temperature of 290 K, a measurement bandwidth of 10 kHz and a low noise receiving system with a system noise temperature of 40 K. The waveguide horn gain (dBi) taken from the data sheet and the transmitted power required for equal received signal power and noise power are shown in Table. 1. The four frequencies chosen are associated with minima in the noise powers shown in Fig.8 and are examples of the widest range of received noise powers in the reverberation chamber across the 1 GHz to 10 GHz frequency range.

Frequency (GHz)	G_{rx} (dBi)	P (dBm)
1.09	6.0	-97.8
2.56	8.7	-94.2
5.4	9.6	-88.5
8.4	10.7	-84.7

Table 1. Receiving antenna gain and commensurate transmitter powers for received signal power and total noise power equality in the anechoic chamber

B. Signal to Noise Ratio in the Reverberation Chamber

In Section IV.A above the transmitter powers required for equal received signal power and total noise power in the anechoic chamber were calculated. Combining these transmitter powers with the data from Fig.6 allows the signal powers received in the reverberation chamber at each stirrer position for the same transmitter powers to be estimated.

The received noise power at each stirrer position is taken from the data shown in Fig. 9. In Fig.10, Fig. 11, Fig. 12 and Fig. 13 scatter plots showing the estimated signal (S_{RX}) and noise (N_{RX}) powers at each stirrer position are shown.

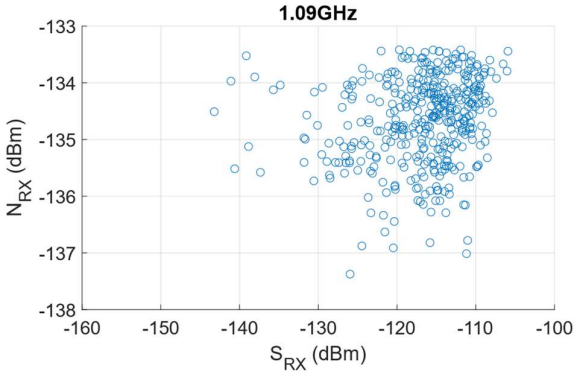

Fig. 10. Scatter plot showing the received signal powers (S_{RX}) and noise powers (N_{RX}) at each stirrer position at 1.09 GHz.

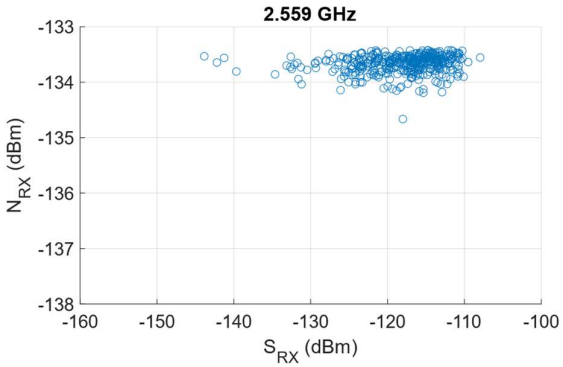

Fig. 11. Scatter plot showing the received signal powers (S_{RX}) and noise powers (N_{RX}) at each stirrer position at 2.559 GHz.

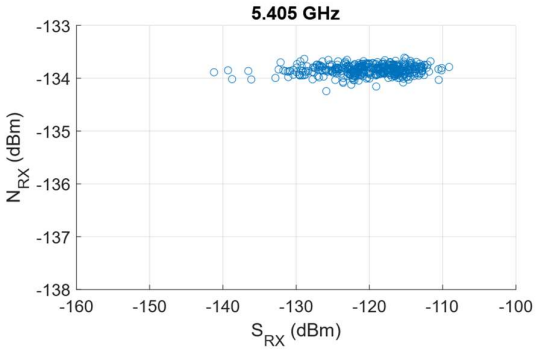

Fig. 12. Scatter plot showing the received signal powers (S_{RX}) and noise powers (N_{RX}) at each stirrer position at 5.405 GHz.

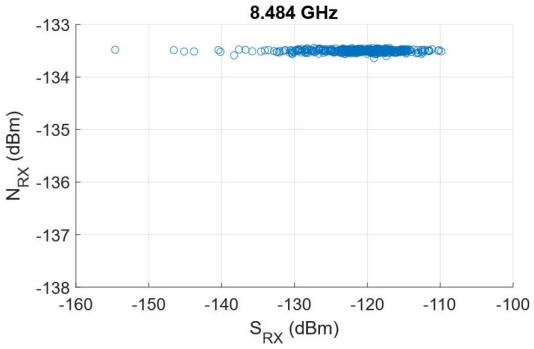

Fig. 13. Scatter plot showing the received signal powers (S_{RX}) and noise powers (N_{RX}) at each stirrer position at 8.484 GHz.

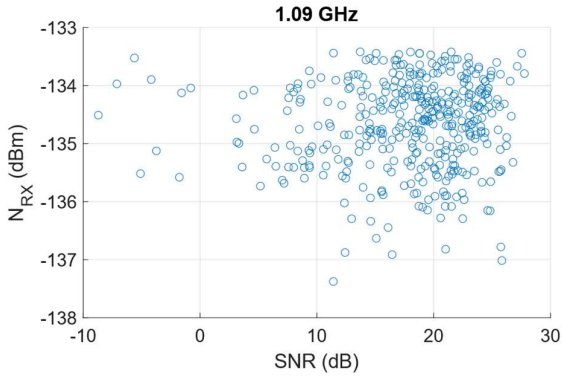

Fig. 14. Scatter plot showing the SNR (dB) and total received noise power (N_{RX}) (dBm) at 1.09 GHz

V. Discussion and Conclusions

For each of the scatter plots in Section IV.B the SNR in the anechoic chamber with the same receiving system and transmitted power would be 0 dB with a total noise power and received signal power of -133 dBm. In the reverberation chamber the estimated range of received signal powers varies by around 45 dB at all frequencies, ranging from -148 dBm to -105 dBm. The enhanced signal strength over that of the anechoic chamber is due to the high Q-factor of the reverberation chamber which, for the York chamber in which the S-parameter measurements were made, varies from 10,000 to 70,000 over the 1 GHz to 10 GHz frequency range. Loading the chamber with a more absorptive EUT would reduce that range. The variability in the total received noise power is dependent on the receiving antenna mis-match variability. It is largest at frequencies where the free space input reflection coefficient is highest; in the example shown here this is at the lower end of the frequency range.

Examination of Fig. 10 to Fig. 13 shows that the overall SNR in the reverberation chamber is dominated by the received signal level at the frequencies where the receiving antenna reflection coefficient is lowest and the corresponding mis-match correction ratio *C* is closest to unity. The variability of the total noise power is small and the noise power values are close to -133 dBm. At frequencies where the mis-match correction ratio *C* is significantly less than unity, the variation in noise power has a significant effect on the SNR values over the range of stirrer positions; in this case, higher SNR values being associated with reduced noise power. Fig. 14 shows the scatter plot of the total received noise power and SNR at the frequency 1.09 GHz where the contribution of the reduced noise power has the greatest effect on the SNR. It can be seen that many of the highest SNR values are associated with the lower noise power values.

The data presented here are for a perfectly matched receiving system. Any receiver input mis-match would alter the mis-match correction ratio, possibly allowing it to exceed unity as demonstrated in [3] and [4]. However, the highest SNR is still associated with the lowest levels of the correction ratio *C*. This is significant when searching for a low-level signal in the reverberation chamber. The data presented here are calculated for a receiving system with a very low input noise temperature of 40 K, equivalent to a NF of 0.6 dB, such as would be used in the search for low-level signals. Using a receiving system with a higher NF reduces the effect of the mis-match correction ratio *C* as can be seen by examination of (6). The assumed ambient temperature of 290 K is the dominant effect in determining the overall noise power when using a receiving system with a very low NF. A lower ambient temperature is advantageous for the detection of low-level signals in both the anechoic and reverberation chamber measurement environments. In all cases presented here, any reduction of the measurement bandwidth *B* simply results in an increase in the SNR values proportional to the bandwidth change. The overall conclusions remain unaltered.

Acknowledgement

For this work Professor Emeritus Marvin is supported by the Leverhulme Foundation Emeritus Fellowship EM-2021-039\4

References

[1] International Electrotechnical Commission, 61000-4-21 ELECTROMAGNETIC COMPATIBILITY (EMC), Part 4: Testing and Measurement Techniques, Section 21: Reverberation Chamber Test Methods. 2011.

[2] International Electrotechnical Commision, 61000-4-22 ELECTROMAGNETIC COMPATIBILITY (EMC), Part 4, Testing and Measurement Techniques, Radiated emission and immunity measurements in fully anechoic rooms (FARs). 2010.

[3] A. C. Marvin & S. J. Bale. "Thermal Noise Measurements in a Reverberation Chamber" in press in IEEE Transactions on Electromagnetic Compatibility Vol 64, No 3, June 2022. Pp. 293-297.

[4] A. C . Marvin & S. J. Bale. "An Experimental Study of the Signal to Noise Ratio of Radiated Emissions in the Presence of Thermal Noise in a Reverberation Chamber". EMC Europe 2022, Gothenburg, Sweden. September 5-8, 2022.

[5] H. T. Friis. "A Note on a Simple Transmission Formula". IRE Proc Vol 34, No 5, May 1946, pp 254 – 256.